ARCHIVES
of
FOUNDRY ENGINEERING

ISSN (2299-2944)

10.24425/afe.2026.158016

Published quarterly as the organ of the Foundry Commission of the Polish Academy of Sciences

Study on Decarburization and Dehydrogenation of Molten Steel under CO_2/Ar Mixed Blowing

Peng Zhao, Chen xiao Li *, Ding guo Zhao, Shu huan Wang, Kai xuan Zhang, Qian qian Gao
College of Metallurgy and Energy, North China University of Science and Technology, Tangshan 063210, Hebei, China
* Corresponding author: E-mail address: lichenxiao34@163.com

Received 21.05.2025; accepted in revised form 09.07.2026; available online 31.08.2026

Abstract

To investigate the application potential of CO_2 in molten steel refining, CO_2/Ar mixed-gas bottom blowing experiments were conducted using a high-temperature tubular furnace. The effects of gas mixing ratio, initial carbon content, blowing flow rate, and refining temperature on the decarburization, oxygen control, and dehydrogenation behaviors of molten steel were systematically studied, and the purification mechanism induced by CO bubbles was analyzed. The results show that CO_2/Ar mixed blowing effectively promotes molten steel decarburization, with the optimal comprehensive purification effect achieved at 1600 ℃ under 50% CO_2–50%Ar conditions. As the initial carbon content increased from 0.15% to 0.65%, the decarburization amount increased from approximately 0.045% to 0.129%. When the blowing flow rate increased from 10 mL/min to 40 mL/min, the decarburization rate increased by approximately 2.21 times. Fine CO bubbles generated by the CO_2–C reaction not only enhanced decarburization, but also reduced the total oxygen content by adsorbing and entraining oxide inclusions. The average total oxygen content stabilized within 32-35 ppm, with the minimum value of 32.7 ppm obtained at 1600 ℃. Meanwhile, CO bubble flotation promoted molten steel dehydrogenation, and the lowest average hydrogen content of 32.2 ppm was achieved at 30 mL/min. The results indicate that CO_2/Ar mixed blowing has promising potential as a novel green refining process for clean steel production with both low reoxidation and deep purification capabilities.

Keywords: CO_2/Ar bottom blowing, Molten steel refining, Decarburization, Oxygen control, Dehydrogenation

1. Introduction

With the increasing demand for high-quality clean steels, the refining process has imposed increasingly stringent requirements on the control of molten steel cleanliness [1]. For high-end steel grades such as tire cord steel, bearing steel, and high-strength steel, the contents of carbon, oxygen, hydrogen, and other elements in molten steel directly affect inclusion control, mechanical properties, and service stability of the materials [2,3]. Therefore, achieving the coordinated control of deep decarburization, oxygen control, and dehydrogenation during the refining process has become an important research direction in modern clean steel production. At present, vacuum refining processes such as RH, VD, and VOD are widely used for molten steel degassing and purification treatment, owing to their effectiveness in reducing the content of gaseous elements in molten steel [4–6]. However, vacuum refining processes generally suffer from disadvantages such as high equipment investment, high energy consumption, and elevated production costs [7–9]. Meanwhile, although the conventional Ar bottom blowing process can improve molten bath flow and mass transfer conditions, it is essentially an inert gas stirring method with limited capability for molten steel decarburization and deep purification [10]. Therefore, the development of novel refining atmospheres that

possess both metallurgical reaction capability and molten bath strengthening effects is of great significance for promoting green and low-carbon metallurgy as well as efficient clean steel production. In recent years, CO_2, as a recyclable oxygen-containing gas, has gradually attracted increasing attention in the metallurgical field. Numerous studies have shown that under high-temperature conditions, CO_2 can react with carbon in molten steel, thereby achieving molten steel decarburization [11–15]. Compared with conventional oxygen decarburization, CO_2 exhibits weaker oxidizing ability, and its reaction process is relatively mild, which can avoid severe oxidation of molten steel under certain conditions. Therefore, it has demonstrated promising application potential in converter steelmaking, electric furnace smelting, and high-temperature melt reactions [16–20]. However, current studies on CO_2 metallurgy mainly focus on decarburization behavior and thermodynamic analysis, while investigations on its molten steel purification effect during the refining process remain relatively limited, especially the systematic studies on the evolution behaviors of oxygen and hydrogen in molten steel and their synergistic purification mechanisms. In fact, a large number of fine CO bubbles generated by the reaction between CO_2 and carbon in molten steel can not only promote the decarburization reaction, but may also enhance molten steel stirring and gas–liquid mass transfer behavior during the bubble flotation process. On the one hand, fine CO bubbles can adsorb and entrain oxide inclusions in molten steel, thereby reducing the total oxygen content of molten steel. On the other hand, the floating process of bubbles can provide escape channels for hydrogen, thus promoting molten steel dehydrogenation. In addition, the Based on this, CO_2/Ar mixed-gas bottom blowing was adopted in this study to systematically investigate the effects of gas mixing ratio, initial carbon content, blowing flow rate, and refining temperature support and process guidance for the application of CO_2 in the molten steel refining process.

2. Experiments

2.1. Test Raw Materials

The raw materials used in the experiments were mainly industrial steel samples obtained from the pre-LF refining process of a steel plant. Approximately 300 g of steel sample was used for each experimental group and remelted prior to the experiments. To minimize the influence of surface oxides on the experimental results, the oxide layer and adhered impurities on the steel sample surface were first removed by grinding with sandpaper before melting, thereby ensuring a clean sample surface. Subsequently, the treated steel samples were loaded into a quartz crucible and placed in the constant-temperature zone of a high-temperature tubular furnace for heating and melting.

2.2. Experimental Equipment and Methods

To control the molten bath atmosphere and reaction conditions during the melting process, a gas mixing tank was installed in the experimental system. Before entering the molten steel, CO_2 and Ar were first premixed in the mixing tank according to the preset ratios, so as to regulate the bottom blowing atmosphere under different CO_2/Ar mixing ratios. The experimental setup and process flow are shown in Fig. 1.

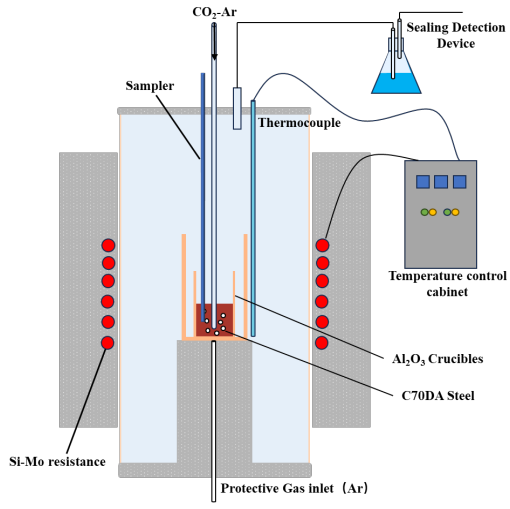

Fig. 1. Experimental apparatus

According to the different experimental parameter settings, the experiments were mainly designed with four variables, including different CO_2/Ar gas mixing ratios, different blowing flow rates, different refining temperatures, and different initial carbon contents, in order to investigate the effects of CO_2/Ar mixed-gas bottom blowing on the decarburization, oxygen control, and dehydrogenation behaviors of molten steel. The specific experimental procedures are as follows:

First, a high-temperature thermocouple was used to calibrate the constant-temperature zone of the tubular furnace. By adjusting the thickness of the furnace bottom plate beneath the crucible, it was ensured that the thermocouple could accurately measure the temperature within the constant-temperature zone. Subsequently, the molten steel composition was prepared according to the experimental scheme, and the quartz crucible was placed in the constant-temperature zone of the furnace. Before the experiment, high-purity Ar was introduced as a protective gas at a flow rate of 1000 mL/min and continuously purged through the furnace tube for 30 min to remove residual air and stabilize the furnace atmosphere. After purging, the heating system was started. When the furnace temperature reached the preset experimental temperature, an Al_2O_3 lance was vertically inserted into the molten steel, with its nozzle positioned close to the bottom of the quartz crucible. The CO_2/Ar mixed gas, with the prescribed mixing ratio and flow rate, was then injected through the submerged nozzle into the bottom region of the molten bath, thereby simulating a laboratory-scale bottom gas injection refining process. During the experiment, molten steel samples were extracted every 10 min using a quartz sampling tube and immediately water-quenched to preserve the instantaneous composition state of the molten steel. After the experiments, the contents of carbon, oxygen, and hydrogen in the molten steel samples were determined using a carbon–sulfur analyzer and an

oxygen–nitrogen–hydrogen analyzer, respectively, in order to investigate the decarburization, oxygen control, and dehydrogenation behaviors of molten steel under different process conditions. The average decarburization rate was calculated from the slope of the linear fitting of carbon content versus refining time for each experimental condition.

3. Experimental Results and Discussion

3.1. Effect of Different Gas Mixing Ratios on the Decarburization Behavior of Molten Steel

To investigate the oxidation behavior of molten steel under different CO_2/Ar mixed-gas atmospheres, laboratory refining experiments were conducted in a high-temperature tubular furnace under Ar protection. The variation of average carbon content in molten steel at different sampling times was measured under different CO_2/Ar mixing ratios, and the results are presented in Fig. 2.

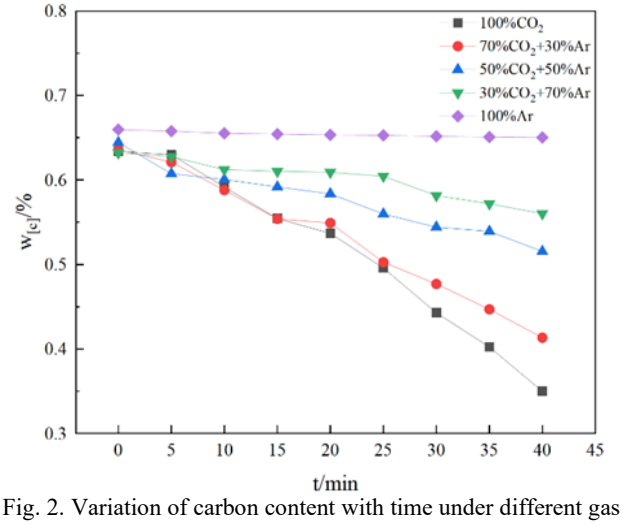

Fig. 2. Variation of carbon content with time under different gas mixing ratios

As shown in Fig. 2, the regulation of the decarburization rate by the CO_2/Ar mixing ratio is essentially the result of the synergistic effect between CO_2 concentration and bubble dynamics. Under the condition of 100% CO_2, the high CO_2 partial pressure significantly increases its dissolution in molten steel, enabling the CO generation rate at the carbon–oxygen reaction interface to reach a maximum. CO molecules rapidly accumulate to form local supersaturation and subsequently trigger heterogeneous nucleation through non-metallic inclusions. Meanwhile, in pure CO_2 blowing, the generated bubble group is free from the dilution effect of Ar, and the continuous increase in CO partial pressure may instead suppress the escape efficiency of CO.

As the Ar proportion increases to 30%–70%, the dual effect of the mixed gas gradually becomes evident. On the one hand, the dilution effect of Ar decreases the CO_2 partial pressure, resulting in reduced CO_2 solubility and effective CO_2 concentration, thereby weakening the driving force for decarburization. On the other hand, Ar bubbles are considered to provide preferential heterogeneous nucleation sites for CO bubble formation, thereby facilitating bubble nucleation. CO molecules may preferentially accumulate at the surface of Ar bubbles, promoting the heterogeneous nucleation and subsequent growth of CO bubbles. The rapid flotation process of these bubbles not only removes the reaction product CO through the Le Chatelier effect, but also enhances gas–liquid interfacial mass transfer through bubble wake-induced disturbance. When the Ar proportion increases to 70%, although the CO_2 partial pressure has been substantially reduced, the abundant nucleation sites and mechanical stirring effect provided by the high-density Ar bubble group partially compensate for the deficiency of oxidizing gas, resulting in a slower decrease in decarburization amount.

Under pure Ar conditions, however, due to the absence of CO_2 participation in the carbon–oxygen reaction, sufficient CO molecules cannot be generated to overcome the critical supersaturation required for nucleation, leading to the failure of the bubble nucleation mechanism and stagnation of the decarburization reaction.

Therefore, gas composition is the primary factor governing the decarburization driving force, with CO_2 mainly controlling the carbon–oxygen reaction, while Ar improves the reaction kinetics through bubble nucleation and molten bath stirring. The dynamic balance between the two ultimately determines the decarburization efficiency.

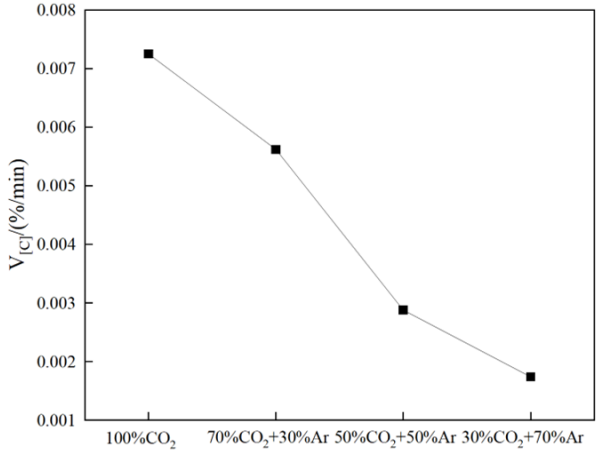

Fig. 3. Variation of decarburization rate under different gas mixing ratios

The study on the effect of different Ar/ CO_2 mixing ratios on decarburization kinetics indicates that the reaction rate between active oxygen [O], generated by the high-temperature decomposition of CO_2, and carbon in the molten bath is regulated by the gas-phase partial pressure. When the Ar proportion increases to 70%, the CO_2 partial pressure decreases significantly, resulting in a reduction in active oxygen concentration and a weakened driving force for decarburization. Under this condition,

the sensitivity of the reaction rate to partial pressure variation decreases. In contrast, under high CO_2 proportion conditions (such as pure CO_2 blowing), the increase in gas–liquid interfacial area accelerates mass transfer during the carbon–oxygen reaction, thereby enhancing the decarburization rate.

3.2. Effect of Different Initial Carbon Contents on the Decarburization Behavior of Molten Steel

In the refining process, the carbon content in the molten bath generally ranges from 0.1% to 0.7%. Therefore, the influence of [C] content on molten bath decarburization behavior must be considered. In this study, high-, medium-, and low-carbon steels were selected for experiments on initial carbon content in order to accommodate the refining characteristics of different steel grades. The variation in carbon content is shown in Fig. 4.

According to the analysis of the data in Fig. 4(a), with increasing reaction time, the decarburization reaction of the mixed gas proceeded in the forward direction under different initial carbon contents, and the carbon content in the molten bath continuously decreased. Furthermore, the variation in decarburization rate under different carbon contents was obtained through fitting analysis, as shown in Fig. 4(b).

As shown in Fig. 4(a), during the refining process, high-carbon steel (0.6%–0.7%) exhibited the largest decarburization amount, reaching approximately 0.129%; medium-carbon steel (0.3%–0.6%) showed a relatively lower decarburization amount of about 0.1037%; while low-carbon steel (<0.25%) presented the lowest decarburization amount, approximately 0.045%. According to Fig. 4(b), the increase in initial carbon content significantly enhanced the decarburization reaction rate, especially within the range of 0.15%–0.5%, where a linear first-order reaction characteristic was observed. This indicates that the rate of the carbon–oxygen reaction directly depends on the variation in molten bath carbon concentration.

When the initial carbon content increased from 0.15% to 0.65%, the chemical driving force of the carbon–oxygen reaction was strengthened, and the probability of contact between carbon atoms and CO_2 increased, thereby accelerating the generation rate of CO molecules at the reaction interface. As the local CO concentration rapidly reached supersaturation, CO molecules preferentially aggregated at the molten steel–inclusion interface or gas-phase boundary defects, triggering heterogeneous nucleation. In the high-carbon steel molten bath (0.6%–0.7%), the large amount of generated CO molecules significantly reduced the critical supersaturation required for bubble nucleation, making CO bubbles more likely to nucleate rapidly at sites with lower interfacial energy, such as the surfaces of Ar bubbles or microscopic inclusions. The enhanced CO bubble generation further promoted gas–liquid mass transfer and facilitated the decarburization reaction.

When the carbon content exceeded 0.5%, although the increase in decarburization rate gradually slowed, the synergistic effect between the reduced viscosity of molten steel and the accelerated CO generation rate under high-carbon conditions further optimized the dynamic process of bubble nucleation and escape. On the one hand, the increase in carbon concentration weakened the viscous resistance of molten steel to bubbles, accelerating bubble detachment. On the other hand, the continuously released CO bubbles enhanced the renewal frequency of the carbon–oxygen reaction interface through mechanical stirring, thereby forming a positive feedback mechanism between carbon–oxygen mass transfer and bubble dynamics, ultimately maximizing the decarburization amount of high-carbon steel.

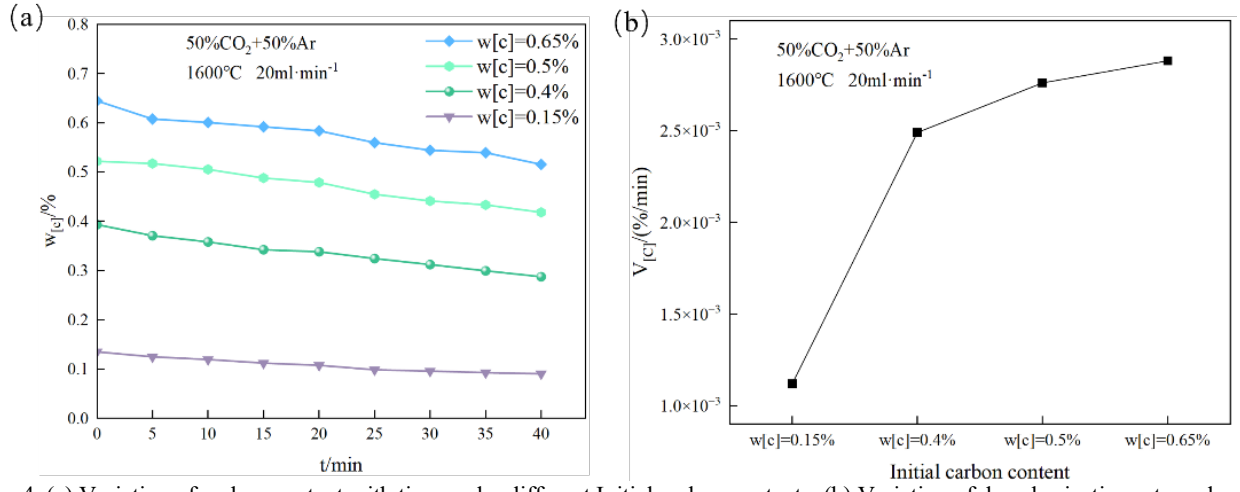

Fig. 4. (a) Variation of carbon content with time under different Initial carbon contents; (b) Variation of decarburization rate under different Initial carbon contents

3.3. Effect of Molten Bath Temperature on the Decarburization Behavior of Molten Steel

Changes in refining temperature directly affect the molten bath state and reaction rate. To ensure that CO_2 can utilize its weak oxidizing property to react with carbon in the molten bath under high-temperature conditions and thereby satisfy refining requirements, it is necessary to investigate the influence of temperature variation on the molten bath decarburization reaction. The variation of carbon content with time at different temperatures is shown in Fig. 5(a). Under different steelmaking temperatures, the carbon content in the molten bath decreased continuously with increasing reaction time. The experimental data were further processed through linear fitting to obtain the variation of decarburization rate at different temperatures, as shown in Fig. 5(b).

Under high-temperature conditions, the increase in refining temperature affects the decarburization reaction rate through a dual mechanism involving both kinetics and thermodynamics. As shown in Fig. 5(b), when the temperature increased from 1550 °C to 1650 °C, according to the Arrhenius effect, the reaction rate constant increased with temperature, resulting in a slight increase in decarburization rate of $0.00015\%\cdot min^{-1}$. However, the dilution effect of Ar in the mixed gas intensified the decrease in CO_2 partial pressure, causing the solubility of CO_2 to decrease significantly with increasing temperature. Consequently, the concentration of effective decarburizing agent in molten steel was reduced, weakening the promoting effect of temperature rise on the reaction rate.

Nevertheless, the high-temperature environment indirectly enhanced the decarburization process by promoting CO bubble nucleation behavior. On the one hand, the diffusion kinetic energy of CO molecules generated by the carbon–oxygen reaction increased at elevated temperatures, making it easier to form local supersaturation at the molten steel–gas interface or on the surfaces of inclusions, thereby promoting heterogeneous nucleation. On the other hand, the increase in temperature significantly reduced the viscosity of molten steel, decreasing the nucleation work required for CO bubbles to detach at the critical size and accelerating bubble generation and escape. The enhancement of bubble dynamics not only continuously removed the reaction product CO through the Le Chatelier effect to maintain the reaction driving force, but also induced molten bath turbulence during bubble escape, further disrupting the gas–liquid interfacial mass transfer boundary layer. This formed a synergistic mechanism of "high-temperature-promoted nucleation and bubble-disturbance-enhanced mass transfer," thereby enabling a slight increase in decarburization rate even under the unfavorable condition of reduced CO_2 solubility.

3.4. Steel Effect of Blowing Flow Rate on the Decarburization Behavior of Molten Steel

The CO_2 blowing flow rate is an important parameter affecting the decarburization reaction in molten steel during the steelmaking process. The blowing flow rate directly influences the molten bath dynamic conditions, thereby affecting the element contents in the molten bath. Based on the variation data of carbon content, the change in carbon content under different blowing flow rates was plotted, as shown in Fig. 6(a).

Different blowing flow rates have a significant influence on the carbon content and decarburization rate of molten steel. With increasing flow rate, the carbon content decreases more rapidly, and the decarburization rate correspondingly increases. According to the experimental data shown in Fig. 6(a), during bottom blowing of mixed gas ($50\%CO_2 + 50\%Ar$) at 1600 °C, when the blowing flow rate increased from 10 $mL\cdot min^{-1}$ to 40 $mL\cdot min^{-1}$, the mass fraction of carbon in the molten steel system exhibited a significant decreasing trend with time.

As shown in Fig. 6(b), increasing the blowing flow rate enhanced the turbulence intensity at the molten steel–gas interface, thereby increasing the decarburization reaction rate. According to the two-film theory of multiphase reaction systems, the increase in gas flow velocity effectively reduced the thickness of the gas–liquid boundary layer and significantly improved the mass transfer coefficient of CO_2 toward molten steel, thus promoting the decarburization reaction. Meanwhile, the heterogeneous bubble nucleation mechanism induced by fluctuations in molten steel static pressure further accelerated the carbon–oxygen reaction process. When the gas flow rate increased to 40 $mL\cdot min^{-1}$, the dynamic fluid disturbance generated by the ascending Ar bubble swarm destabilized the local static pressure field in the molten steel, promoting the preferential aggregation and nucleation of CO molecules at defects on the gas–liquid interface and significantly reducing the activation energy required for bubble formation.

The increase in blowing flow rate enhanced gas–liquid mass transfer and promoted CO bubble formation, thereby accelerating the decarburization reaction. As a result, the decarburization rate reached approximately 2.21 times that obtained under the low-flow-rate condition. Overall, the experimental results indicate that gas composition primarily determines the decarburization driving force, whereas the blowing flow rate and refining temperature mainly regulate the reaction kinetics and gas–liquid mass transfer, jointly determining the overall decarburization performance.

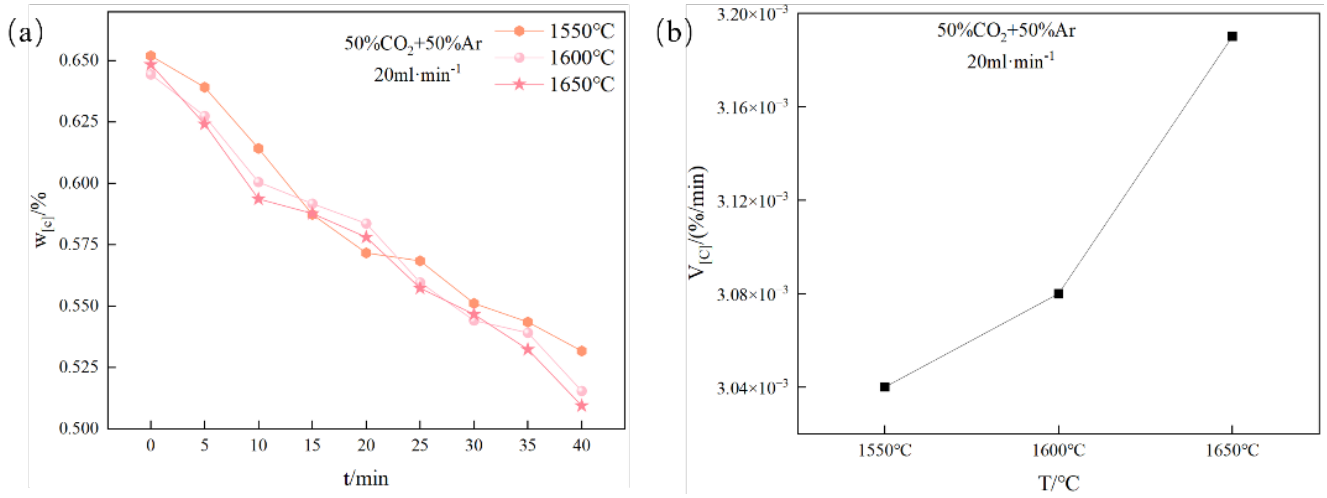

Fig. 5. (a) Variation of carbon content with time at different temperatures; (b) Variat ion of decarburization rate at different temperatures

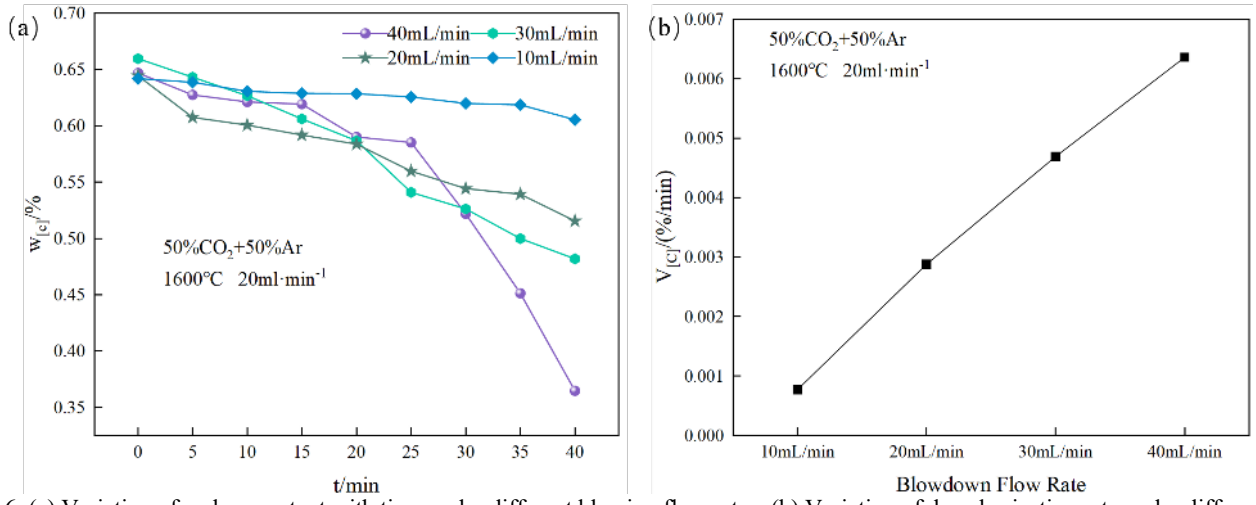

Fig. 6. (a) Variation of carbon content with time under different blowing flow rates; (b) Variation of decarburization rate under different blowing flow rates

3.5. Effect of CO_2/Ar Blowing on the Oxygen and Hydrogen Behaviors of Molten Steel

Based on the decarburization results presented in Section 3.1, the 50%CO_2–50%Ar condition exhibited the most favorable overall refining performance among the investigated gas compositions. Compared with pure CO_2 blowing, it maintained a high decarburization efficiency while effectively suppressing excessive oxidation of the molten steel. In contrast, lower CO_2 proportions (30%CO_2 and 70%Ar) reduced the decarburization driving force because of the decreased CO_2 partial pressure, whereas pure Ar blowing exhibited only a negligible decarburization effect due to the absence of a carbon–oxygen reaction. Therefore, considering both decarburization performance and oxidation control, the 50%CO_2–50%Ar condition was selected as the representative operating condition for the subsequent investigation of oxygen and hydrogen behaviors. Under this condition, the influences of blowing flow rate and refining temperature on the purification behavior of molten steel were further evaluated.

Fig. 7 shows the variation of element contents in molten steel under different blowing flow rates, in which Fig. 7(a) presents the variation curves of oxygen content with time. The results indicate that under all blowing flow rate conditions, the oxygen content in molten steel continuously decreased, and the reduction trend gradually became stable with increasing blowing flow rate.

The convergence of oxygen content with increasing flow rate is mainly attributed to the following reasons: a higher blowing flow rate enhances the stirring intensity of the molten bath, resulting in more sufficient interfacial interaction between CO bubbles and molten steel, which is beneficial for the entrainment and removal of oxide inclusions. Meanwhile, a higher flow rate can maintain a stable CO_2–C reaction intensity, thereby promoting continuous decarburization and reducing the oxygen activity in molten steel. When the flow rate is further increased to

a certain level, the enhancement of stirring and the bubble entrainment effect gradually approach saturation, and thus the decrease in oxygen content becomes progressively stabilized.

Fig. 7(b) shows the variation behavior of hydrogen content in molten steel under different blowing flow rate conditions. Compared with the initial hydrogen content, the CO_2–Ar mixed gas exhibited a certain dehydrogenation effect at all flow rates. However, with increasing blowing flow rate, the dehydrogenation effect gradually weakened, as reflected by the reduced decrease in hydrogen content. The main reason for this trend is that although a higher blowing flow rate enhances molten bath stirring, it simultaneously shortens the residence time of CO bubbles in molten steel, thereby reducing the mass transfer efficiency between the bubbles and dissolved hydrogen in molten steel and weakening the ability of bubbles to carry hydrogen out of the melt. In addition, intensified surface fluctuation under high flow rate conditions may promote the reabsorption of hydrogen from the molten steel–gas interface, resulting in a decrease in overall dehydrogenation efficiency.

Fig. 8(a) shows the variation behavior of the average total oxygen content in molten steel under different bottom blowing flow rates. It can be observed that with increasing blowing flow rate, the average total oxygen content first decreased significantly and then gradually stabilized within the range of approximately 32–35 ppm. This indicates that within the low-flow-rate range, increasing the bottom blowing flow rate can effectively enhance molten bath stirring and the entrainment effect of CO bubbles, thereby significantly reducing the total oxygen level in molten steel. However, when the flow rate increased beyond a certain range, the number of bubbles and the entrainment efficiency gradually approached saturation, resulting in no further significant change in the average total oxygen content and exhibiting a relatively stable fluctuation range.

Fig. 8(b) presents the variation trend of the average hydrogen content in molten steel under different bottom blowing flow rate conditions. It can be observed that with increasing blowing flow rate, the average hydrogen content in molten steel first decreased and then increased, reaching the minimum value of 32.2 ppm at a flow rate of 30 mL/min. The occurrence of this optimal dehydrogenation point is mainly attributed to the fact that under a moderate blowing flow rate, the CO bubbles generated by the CO_2–C reaction possess relatively long residence times and favorable interfacial mass transfer conditions, which facilitate the diffusion of dissolved hydrogen toward the bubble interface and its removal together with bubble flotation, thereby achieving higher dehydrogenation efficiency.

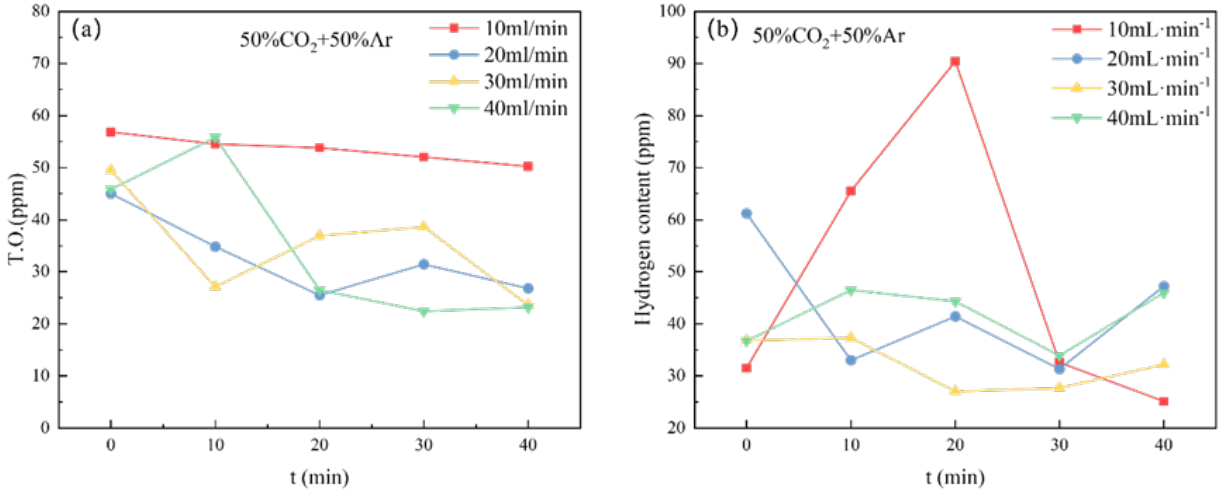

Fig. 7. Variation of element contents in molten steel under different blowing flow rates: (a) variation of oxygen content; (b) variation of hydrogen content

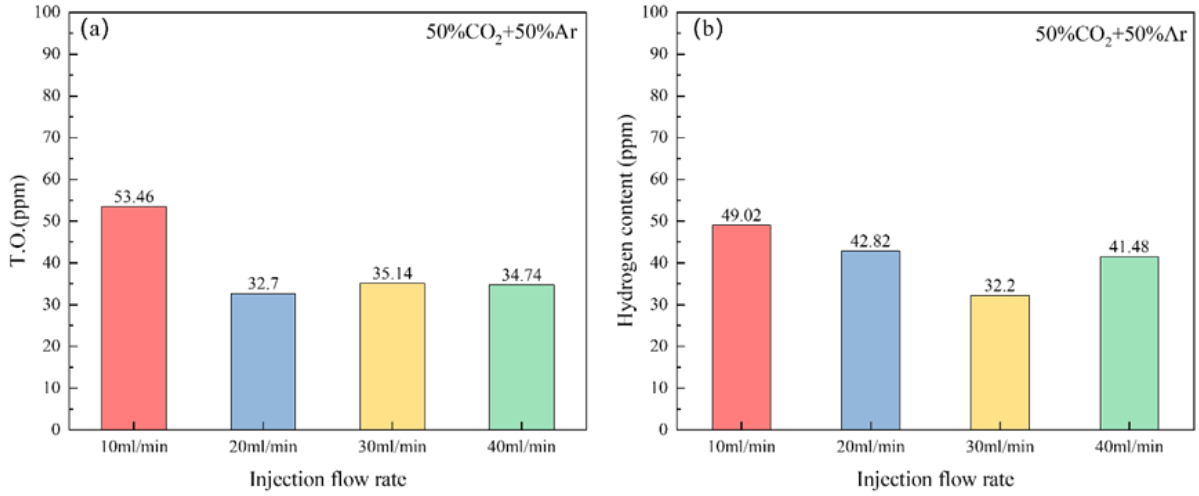

Fig. 8. Variation of average element contents in molten steel under different bottom blowing flow rates: (a) oxygen content; (b) hydrogen content

When the flow rate is lower than this range, the limited number of bubbles and insufficient stirring effect restrict the dehydrogenation efficiency. In contrast, when the flow rate continues to increase, although the amount of generated bubbles increases, the flotation velocity of bubbles becomes faster and the residence time becomes shorter, resulting in a reduced capacity of bubbles to carry hydrogen. Meanwhile, intensified molten bath surface disturbance under high flow rate conditions may promote hydrogen absorption at the gas–steel interface, thereby weakening the overall dehydrogenation effect. Therefore, the average hydrogen content in molten steel exhibits a trend of first decreasing and then increasing, achieving the optimal dehydrogenation effect under moderate flow rate conditions.

Fig. 9 shows the variation of element contents in molten steel under different refining temperature conditions, in which Fig. 9(a) presents the evolution behavior of oxygen content with time. It can be observed that under the condition of 1600 ℃, the final total oxygen content of molten steel is significantly lower than those under 1550 ℃ and 1650 ℃. This is mainly attributed to the fact that at 1600 ℃, the kinetic conditions of the decarburization reaction and the flotation behavior of bubbles reach a relatively coordinated state, enabling both the CO_2–C reaction rate and the capability of CO bubbles to float upward and entrain inclusions to remain within an appropriate range, thereby allowing oxide inclusions to be removed more efficiently.

In contrast, at 1550 ℃, the relatively low temperature results in higher molten steel viscosity and restricted carbon–oxygen reaction kinetics, leading to insufficient CO bubble generation and weaker stirring effects. Consequently, the efficiency of inclusion entrainment and removal is reduced, resulting in a relatively high final total oxygen content. At 1650 ℃, although the elevated temperature promotes the carbon–oxygen reaction, excessively high temperatures significantly reduce the oxygen activity coefficient of molten steel and enhance the decomposition tendency of CO_2, causing more oxygen to enter the molten steel. Meanwhile, excessively rapid bubble generation and flotation shorten the residence time of bubbles in molten steel, thereby reducing the effectiveness of oxide inclusion entrainment. Therefore, 1600 ℃ represents the optimal temperature range balancing reaction kinetics and flow characteristics, resulting in the lowest final total oxygen content.

Fig. 9(b) presents the evolution behavior of hydrogen content in molten steel under different refining temperature conditions. Overall, the hydrogen content in molten steel showed a decreasing trend with the progress of the refining process. However, the final hydrogen contents differed significantly under different temperature conditions: the lowest final hydrogen content was obtained at 1550 ℃, followed by 1650 ℃, while the highest final hydrogen content was observed at 1600 ℃. At 1550 ℃, although the temperature was relatively low, the higher viscosity of molten steel reduced the flotation velocity of bubbles, thereby prolonging the residence time of CO bubbles in molten steel and enhancing the diffusion and removal efficiency of hydrogen toward the bubble interface. Meanwhile, the lower temperature suppressed the tendency of hydrogen reabsorption from the gas–steel interface, resulting in the best overall dehydrogenation effect. In contrast, at 1650 ℃, the elevated temperature significantly accelerated the CO_2–C reaction rate and generated a large number of CO bubbles, which favored dehydrogenation. However, the excessively high temperature also enhanced the diffusion and redissolution ability of hydrogen in molten steel, causing the final dehydrogenation effect to be slightly inferior to that at 1550 ℃. At 1600 ℃, the carbon–oxygen reaction proceeded moderately and the bubble residence time was relatively short, while hydrogen exhibited a relatively high dissolution driving force within this temperature range. As a result, the dehydrogenation mechanism was not fully developed, leading to obvious fluctuations in the final hydrogen content.

Fig. 10(a) shows the variation behavior of the average oxygen content in steel under different refining temperatures. With increasing refining temperature, the average total oxygen content first decreased and then increased, reaching the minimum value of 32.7 ppm at 1600 ℃. This result indicates that at approximately 1600 ℃, the thermodynamic equilibrium between dissolved oxygen and oxide inclusions in molten steel is most favorable for reducing the total oxygen level, and the kinetics of inclusion

generation, dissolution, and migration are better coordinated within this temperature range. However, when the temperature further increased above 1650 ℃, the solubility of oxygen in molten steel increased and the interfacial oxidation reaction was accelerated under high-temperature conditions, resulting in a renewed increase in total oxygen content. Based on the above analysis, 1600 ℃ can be regarded as the optimum refining temperature for achieving superior oxygen control and inclusion stability under the present process conditions.

Fig. 10(b) presents the variation behavior of the average hydrogen content in steel under different refining temperatures. It can be observed that with increasing refining temperature, the average hydrogen content first increased slightly and then gradually stabilized. However, the overall variation range was relatively small, remaining within approximately 5–6 ppm.

The main reason for this behavior is that temperature has a significant influence on the solubility of hydrogen in molten steel. As the temperature increases, the solubility of hydrogen in molten steel also increases, making the molten steel more susceptible to hydrogen absorption and resulting in a slight increase in hydrogen content during the initial stage. However, within the higher temperature range, the dissolution and escape processes gradually reach a new dynamic equilibrium, causing the hydrogen content to remain at a relatively stable level. Therefore, within the temperature range investigated in this study, the influence of refining temperature on the average hydrogen content in molten steel is relatively limited.

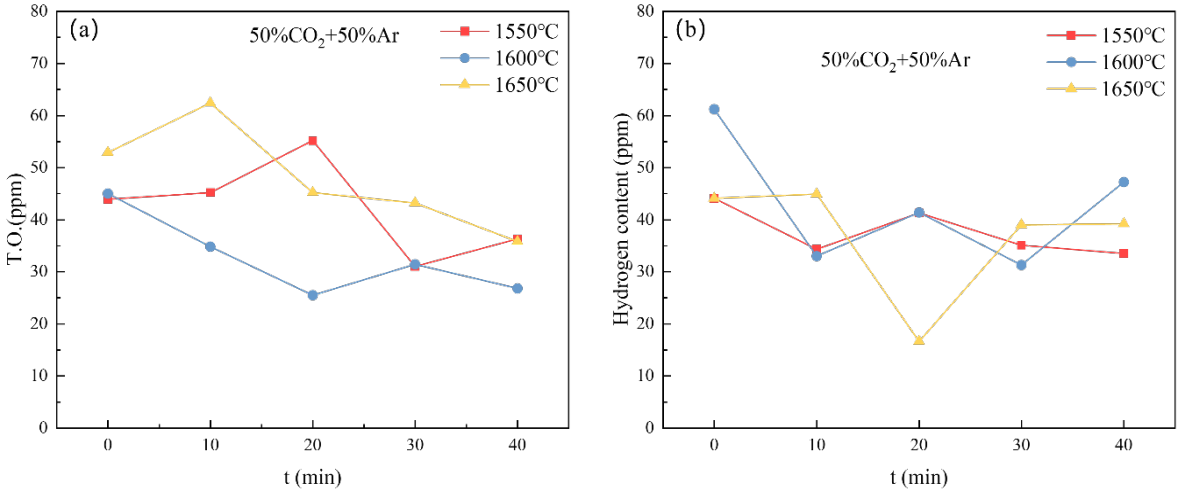

Fig. 9. Variation of element contents in molten steel under different refining temperatures: (a) variation of oxygen content; (b) variation of hydrogen content

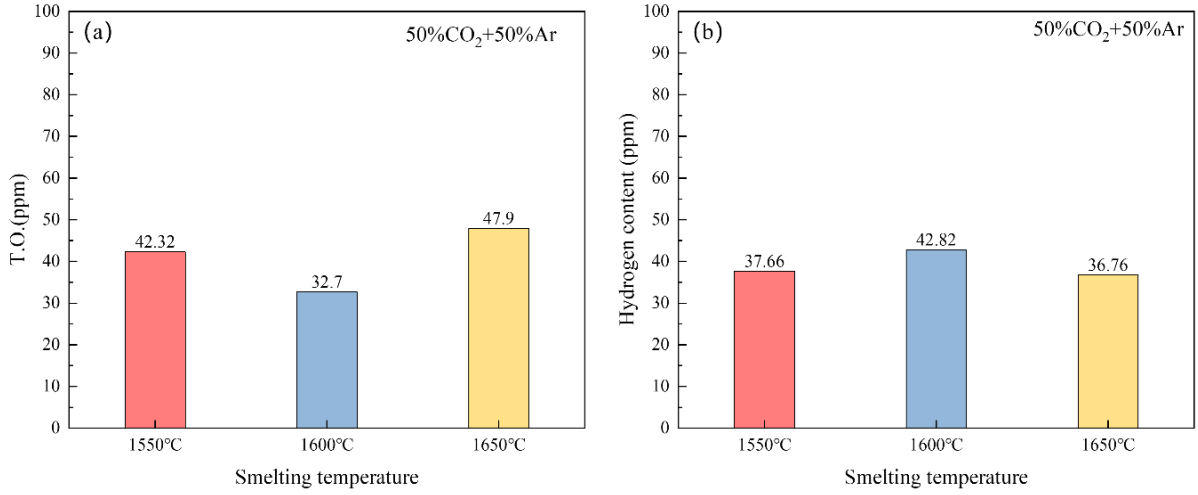

Fig. 10. Variation of average element contents in molten steel under different refining temperatures: (a) oxygen content; (b) hydrogen content

4. Conclusions

1) CO_2/Ar mixed-gas bottom blowing can effectively promote molten steel decarburization, in which CO_2 provides the driving force for the carbon–oxygen reaction, while Ar enhances gas–liquid mass transfer behavior by improving molten bath stirring and bubble nucleation conditions. Under the condition of 50%CO_2–50%Ar, molten steel exhibited a superior decarburization effect. As the initial carbon content increased from 0.15% to 0.65%, the decarburization amount increased from approximately 0.045% to 0.129%, indicating that the proposed process is applicable to molten steel with different initial carbon levels.
2) Blowing flow rate and refining temperature have significant effects on the decarburization kinetics of molten steel. When the blowing flow rate increased from 10 mL/min to 40 mL/min, the decarburization rate increased by approximately 2.21 times. As the refining temperature increased from 1550 ℃ to 1650 ℃, the decarburization rate showed an increasing trend, among which molten steel exhibited the optimal comprehensive decarburization and purification effect at 1600 ℃.
3) A large number of fine CO bubbles generated by the reaction between CO_2 and carbon in molten steel can effectively adsorb and entrain oxide inclusions, thereby reducing the total oxygen content of molten steel. With increasing blowing flow rate, the average total oxygen content gradually decreased and stabilized within the range of 32–35 ppm, among which the minimum total oxygen content reached 32.7 ppm at 1600 ℃, indicating that CO_2 bottom blowing did not cause significant oxygen enrichment in molten steel.
4) The nucleation and flotation process of CO bubbles in molten steel can provide escape channels for hydrogen, thereby achieving molten steel dehydrogenation. Under the condition of 30 mL/min, the average hydrogen content in molten steel reached the minimum value of 32.2 ppm, whereas excessively high blowing flow rates reduced the dehydrogenation efficiency due to the shortened residence time of bubbles.

Although the present study was conducted at the laboratory scale, the proposed CO_2/Ar mixed-gas blowing process demonstrates promising potential for industrial secondary refining. The results suggest that the 50%CO_2–50%Ar condition is particularly suitable for refining processes requiring a balance between decarburization efficiency and oxidation control, especially during the secondary refining stage of clean steel production. Compared with conventional Ar bottom blowing, the proposed process provides a promising approach for improving molten steel purification while promoting efficient CO_2 utilization. Further studies combining physical modeling and CFD simulations will be carried out to evaluate its industrial-scale application.

Acknowledgements

The work was supported by Hebei Province Innovation Ability Improvement Plan (No. 26361004D);Hebei Provincial Natural Science Foundation (E2026209004).

References

[1] Wang, C., Tang, W., Zhang, J., Huang, J., Shen, K., Chen, J. & Liu, Q. (2023). Effect of low basicity refining slag on evolution and removal of oxide inclusions in 55SiCrA spring steel. *Journal of Iron and Steel Research International*. 30(9), 1755-1768. DOI: 10.1007/s42243-023-00941-5.
[2] Wang, Z. & Bao, Y. (2024). Development and prospects of molten steel deoxidation in steelmaking process. *International Journal of Minerals, Metallurgy and Materials*. 31(1), 18-32. DOI: 10.1007/s12613-023-2740-4.
[3] Cheng, G., Zhang, L., Ren, Y., Yang, W., Zhao, X. & Wang, G. (2021). Evolution of nonmetallic inclusions with varied argon stirring condition during vacuum degassing refining of a bearing steel. *Steel Research International*. 92(1), 2000364, 1-13. DOI: 10.1002/srin.202000364.
[4] Ling, H. & Zhang, L. (2018). Investigation on the fluid flow and decarburization process in the RH process. *Metallurgical and Materials Transactions B*. 49(5), 2709-2721. DOI: 10.1007/s11663-018-1319-3.
[5] Sun, W., Wang, Q., Zhou, Y. & Wu, J. (2020). Material and energy flows of the iron and steel industry: Status quo, challenges and perspectives. *Applied Energy*. 268, 114946, 1-15. DOI: 10.1016/j.apenergy.2020.114946.
[6] Lin, L. & Zeng, J. (2021). Consideration of green intelligent steel processes and narrow window stability control technology on steel quality. *International Journal of Minerals, Metallurgy and Materials*. 28(8), 1264-1273. DOI: 10.1007/s12613-020-2246-2.
[7] Park, Y. & Yi, K. (2003). A new numerical model for predicting carbon concentration during RH degassing treatment. *Iron and Steel Institute of Japan International*. 43(9), 1403-1409. DOI: 10.2355/isijinternational.43.1403.
[8] Toshihiro, K., Kenichiro, M., Ryouji, T., Shozo, M. & Katsuhiko, T. (1996). Mathematical model for nitrogen desorption and decarburization reaction in vacuum degasser. *Iron and Steel Institute of Japan International*. 43(9), 395-401. DOI: 10.2355/isijinternational.36.395.
[9] Peng, K., Liu, C., Zhang, L. & Sun, Y. (2022). Numerical simulation of decarburization reaction with oxygen blowing during RH refining process. *Metallurgical and Materials Transactions B*. 53(4), 2004-2017. DOI: 10.1007/s11663-022-02519-0.
[10] Huang, Y., Cheng, G., Wang, Q., Li, S. & Dai, W. (2020). Mathematical model for decarburization of ultra-low carbon steel during RH treatment. *Ironmaking and Steelmaking*. 47(6), 655-664. DOI: 10.1080/03019233.2019.1567999.
[11] Han, B., Gao, C., Li, Y., Liu, D., Wei, G. & Zhu, R. (2024). Energy saving analysis for CO2–O2 mixed injection technology in converter steelmaking. *Journal of Iron and*

Steel Research International. 31(5), 1095-1103. DOI: 10.1007/s42243-023-01170-6.
[12] Zhang, F., Hong, L. & Xu, Y. (2024). Prospects for green steelmaking technology with low carbon emissions in China. *Carbon Energy*. 6(2), e456, 5-28. DOI: 10.1002/CEY2.456.
[13] Medeiros, G., Carbajal Ccoyllo, M., De Siqueira, R. Ghosh, A. (2026). Alternative carbon sources as foaming agents for electric arc furnace steelmaking slags: a comprehensive review. *Minerals*. 16(2), 152, 1-22. DOI: 10.3390/min16020152.
[14] Dong, W., Xu, A., Zhao, C., Ji, C., Li, H., Hao, N., Zhou, H., Xia, T. & Zhu, R. (2023). Reaction mechanism of bottom blowing CO_2 with molten steel in converter. *ISIJ International*. 63(5), 846-853. DOI: 10.2355/isijinternational.ISIJINT-2022-466.
[15] Fan, Y., Yang, Q., Matsuura, H. & Hu, X. (2025). Decarburization and desilication behavior by CO2–O2 mixed gas injection in Fe-C-(Si) molten alloys. *ISIJ International*. 65(13), 2055-2063. DOI: 10.2355/isijinternational.ISIJINT-2024-353.
[16] Zhou, Y., Wei, G. & Zhu, R. (2022). Theoretical analysis and experimental study of the application of CO2in the smelting of 410S stainless steel. *Journal of CO2 Utilization*. 60, 102016, 1-9. DOI: 10.1016/j.jcou.2022.102016.
[17] Wei, G., Zhu, R., Wu, X., Dong, K., Yang, L. & Liu, R. (2018). Technological innovations of carbon dioxide injection in EAF-LF steelmaking. *The Journal of The Minerals, Metals & Materials Society (TMS)*. 70(6), 969-976. DOI: 10.1007/s11837-018-2814-3.
[18] Dong, K., Zhu, R., Liu, R., Wang, H. & Zhou, C. (2014). Influence of bottom blowing CO2 in LF on molten steel quality and erosion of ventilated bricks. *Chinese Journal of Engineering*. 36(S1), 226-229.
[19] Wu, W., Zhu, R., Wang, H., Wang, C. & Wei, G. (2022). Reaction mechanism of CO/CO2 with low-carbon aluminium-killed molten steel during the ladle furnace (LF) refining process. *Ironmaking & Steelmaking*. 49(2), 147-159. DOI: 10.1080/03019233.2021.1972738.
[20] Wang, H., Zhu, R., Wang, X. & Li, Z. (2017). Utilization of CO2 in metallurgical processes in China. *Mineral Processing and Extractive Metallurgy*. 126(1-2), 47-53. DOI: 10.1080/03719553.2016.1255401.